THE JOURNAL OF BIOLOGICAL CHEMISTRY VOL. 281, NO. 47, pp. 36303–36316, November 24, 2006

Microtubules Support Production of Starvation-induced Autophagosomes but Not Their Targeting and Fusion with Lysosomes*[S]

Received for publication, July 24, 2006, and in revised form, September 7, 2006 Published, JBC Papers in Press, September 8, 2006, DOI 10.1074/jbc.M607031200

Ephraim Fass[‡1], **Elena Shvets**[‡1], **Ilan Degani**[‡], **Koret Hirschberg**[§], **and Zvulun Elazar**[‡2]

From the [‡]*Departments of Biological Chemistry and Chemical Physics, Weizmann Institute of Science, Rehovot, 76100 and the* [§]*Department of Cell and Developmental Biology, Sackler Faculty of Medicine, Tel-Aviv University, Ramat-Aviv 69978, Israel*

Autophagy is a major catabolic pathway in eukaryotic cells whereby the lack of amino acids induces the formation of autophagosomes, double-bilayer membrane vesicles that mediate delivery of cytosolic proteins and organelles for lysosomal degradation. The biogenesis and turnover of autophagosomes in mammalian cells as well as the molecular mechanisms underlying induction of autophagy and trafficking of these vesicles are poorly understood. Here we utilized different autophagic markers to determine the involvement of microtubules in the autophagic process. We show that autophagosomes associate with microtubules and concentrate near the microtubule-organizing center. Moreover, we demonstrate that autophagosomes, but not phagophores, move along these tracks en route for degradation. Disruption of microtubules leads to a significant reduction in the number of mature autophagosomes but does not affect their life span or their fusion with lysosomes. We propose that microtubules serve to deliver only mature autophagosomes for degradation, thus providing a spatial barrier between phagophores and lysosomes.

Autophagy is an evolutionarily conserved lysosomal pathway involved in degradation of long lived proteins and cytoplasmic organelles. This process, which is essential for normal turnover of cellular compartments, is up-regulated in response to nutrient starvation. Autophagy starts with the sequestration of cytoplasmic constituents, including organelles such as mitochondria, by a membrane sac known as the isolation membrane (phagophore). Closure of the isolation membrane results in the formation of a double-bilayer membrane vesicle, called the autophagosome (1). Following movement and targeting to lysosomes, the autophagosome outer membrane fuses with the lysosome/vacuole, releasing a single membrane vesicle (autophagic body) into this compartment to generate an autolysosome. Finally, the sequestered contents and the inner membrane are degraded by lysosomal hydrolases. The exact origin of autophagosomes is yet unknown. Recently, however, *de novo* formation by nucleation, *i.e.* assembly and elongation of small membrane structures, has been proposed (2, 3).

The molecular mechanism underlying autophagy was first characterized in the yeast *Saccharomyces cerevisiae* as a model system (4, 5). These studies led to the identification of a novel set of Atg (autophagy-related) factors, some of which are evolutionarily conserved (6–9). Two ubiquitin-like conjugation systems, Atg12 and Atg8, participate in the early stages of autophagy (5). Atg12p is conjugated to Atg5p by Atg7p, an ubiquitin-activating-like enzyme, and by Atg10p, a ubiquitin-conjugating enzyme. The resultant Atg5/12p conjugate, in complex with Atg16, associates with the autophagic membrane and detaches from it immediately upon completion of autophagosome formation (10–12).

The other ubiquitin-like protein, Atg8p, is first cleaved by Atg4p, a specific cysteine protease, thereby exposing a glycine residue (13). Atg8p is then activated by Atg7p, the same ubiquitin-activating enzyme that activates Atg12p, and by Atg3p, a ubiquitin-conjugating enzyme specific for Atg8p (13). Finally, the C-terminal glycine of Atg8p is conjugated via an amide bond to the amino group of the lipid phosphatidylethanolamine (14). The yeast Atg8p is highly homologous to several mammalian proteins, including MAP1-LC3 (LC3), GATE-16, and GABARAP (15–17). The modification of LC3 at its C terminus, like that of Atg8p, is an essential step for the formation of autophagosomes (10, 18). The mammalian Atg4B protease has been recently reported to cleave LC3, exposing its C-terminal glycine 120 (19). This form of LC3, termed LC3-I, is further modified into a membrane-bound form, LC3-II, by the mammalian Atg7p and Atg3p (2, 20). Although implicated in different intracellular membrane trafficking pathways, all three mammalian homologues of Atg8p are processed by Atg4p proteases and by Atg7p and Atg3p conjugation machineries (19, 21, 22) to generate the membrane-bound form (19). LC3 has been shown to be incorporated specifically into autophagic vesicles under conditions that induce autophagy, thus serving as the first *bona fide* marker for autophagosomes in mammalian cells (18, 23, 24).

Despite significant progress in identifying the molecular components that participate in autophagy, little is known about intracellular routes and dynamics of autophagosomes in mammals. Hence, the kinetics of autophagosome formation and

* This work was supported in part by the Israel Science Foundation, the United States-Israel Binational Science Foundation, and by the Weizmann Institute Minerva Center. The costs of publication of this article were defrayed in part by the payment of page charges. This article must therefore be hereby marked "*advertisement*" in accordance with 18 U.S.C. Section 1734 solely to indicate this fact.

[S] The on-line version of this article (available at http://www.jbc.org) contains supplemental Figs. 1 and 2 and videos 1–4.

[1] Both authors contributed equally to this work.

[2] An incumbent of the Sholimo and Michla Tomarin Career Development Chair of Membrane Physiology. To whom correspondence should be addressed. Tel.: 972-8-9343682; Fax: 972-8-9344112; E-mail: bmzevi@wicc.weizmann.ac.il.

delivery, their exact en route movement to lysosomes, and the rate-limiting steps in this process remain unclear. The involvement of microtubules in autophagy in mammalian cells is under a considerable debate. Treatment of cells with vinblastine, a microtubule-depolymerizing drug, has been found in many studies to increase the number of autophagosomes (25–28) and the level of LC3-II (18, 27). This accumulation was viewed in some reports (25) as a failure of microtubules to facilitate assembly and fusion of autophagosomes with the lysosomes. In contrast to this view, in Ehrlich ascites cells, vinblastine did not prevent the entry of hydrolases to autophagosomes (26) but rather accelerated the rate of autophagosome formation (29). Studies using other microtubule-depolymerizing agents, such as nocodazole or colchicine, were also inconsistent with these findings. Hence, nocodazole has been reported to elevate the number of autophagosomes and inhibit autophagy-mediated protein degradation in normal rat kidney cells (30). Likewise, most recently it has been reported that vinblastine as well as nocodazole inhibit fusion of autophagosomes with endosomes (27) suggesting that intact microtubules contribute to autophagosome targeting. Others have shown, however, that nocodazole had no effect on fusion of autophagosomes with lysosomes (29). Consistently, Kabeya *et al.* (18) reported that nocodazole or colchicine (but not vinblastine) does not elevate the level of autophagosomes.

In this study, we utilized different autophagic markers to identify phagophores, autophagosomes, and autolysosomes under normal growth and starvation conditions. We found that autophagosomes, unlike phagophores, associate with and move along microtubules. Our data indicate that intact microtubules are not essential for targeting and fusion with lysosomes. Moreover, autophagosomes can be formed in the absence of intact microtubules but to a significantly lower extent. We propose that microtubules facilitate autophagosome formation and serve to direct mature autophagosomes for degradation in lysosomes.

EXPERIMENTAL PROCEDURES

Antibodies and Reagents—Minimal essential medium (MEMα),[3] Earle's balanced salt solution (EBSS), valine-free MEMα, and fetal calf serum (FCS) were obtained from Biological Industries (Beit Haemek Laboratories, Israel). Nocodazole, paclitaxel (taxol), and bafilomycin A1 (Baf A) were provided by Sigma. L-[U-^{14}C]Valine was obtained from Amersham Biosciences. The following antibodies were used: mouse monoclonal anti-α-tubulin and anti-γ-tubulin (Sigma); rabbit polyclonal anti-Atg16 was a kind gift of Noboru Mizushima (Department of Cell Biology, National Institute for Basic Biology, Okazaki, Japan); mouse monoclonal anti-LAMPI (Developmental Studies Hybridoma Bank, University of Iowa); mouse monoclonal anti-green fluorescence protein (GFP) (Babco); rhodamine-conjugated goat anti-mouse IgG; Cy^{TM}5-conjugated donkey anti-mouse IgG; Texas Red-conjugated donkey anti-rabbit IgG (Jackson ImmunoResearch); and horseradish peroxidase-coupled goat antibody against mouse IgG (Bio-Rad). LysoTracker Red DND-99 was obtained from Molecular Probes. pEYFP-Atg5 was a kind gift of Noboru Mizushima. Anti-LC3 antibody was produced by immunization of a rabbit with a peptide corresponding to the 14 amino acids of the N terminus of LC3 with an additional cysteine (PSEKTFKQRRTFEQC).

DNA Construction—DNA encoding human LC3 was obtained by PCR from the total cDNA of LNCaP cells with LC3 sense primer 5′-CAACAAGCTTCGATGCCGTCGGAGAAGACC-3′ and LC3 antisense primer 5′-CAATAGATCTCGAGCGGCCGCTTACACTGACAATTTCATCCCG-3′. To obtain pGFP-LC3, LC3 DNA was cleaved at HindIII and XhoI sites and inserted into the HindIII and SalI sites of pEGFP-C1, a GFP fusion protein expression vector (Clontech). The point mutation for glycine to alanine at position 120 of LC3 ($LC3_{G120A}$) was created by PCR-based site-directed mutagenesis using LC3 sense primer 5′-CAGGAGACGTTCGCGATGAAATTGTCA-3′ and LC3 antisense primer 5′-TGACAATTTCATCGCGGACGTCTCCTG-3′. Cathepsin-D-GFP was constructed by inserting human cathepsin D into the N terminus of pEGFP-N1 (Clontech) at SalI and EcoRI sites.

Cell Culture and Transfection—Chinese hamster ovary (CHO) and HeLa cells were grown on MEMα supplemented with 10% fetal calf serum (FCS) and 1% penicillin/streptomycin (Sigma) at 37 °C in 5% CO_2. Transfection of cells was performed using Lipofectamine reagent (Invitrogen) at a concentration of 4 μl of Lipofectamine/μg of DNA. Stable clones of GFP-LC3-transfected cells were selected in 1 mg/ml geneticin (G418). All the data presented here was derived from at least three different clones of each cell line.

Starvation and Drug Treatment—To obtain starvation conditions, cells were washed three times by PBS and incubated in EBSS medium at 37 °C for different time periods. To examine the recovery of cells from starvation, cells incubated in EBSS for 2 h were transferred to MEMα, 10% FCS for 40 min at 37 °C. In cells treated with nocodazole or taxol, a pretreatment period of 30 min was applied to ascertain that the experiments are carried out following the effect on microtubules. Drugs were applied at the following final concentrations: 5 μg/ml nocodazole, 100 nM wortmannin, 100 nM Baf A, or 20 μM taxol.

Fluorescence Microscopy—CHO cells were plated on sterile coverslips (13 mm diameter) and cultured under the conditions indicated, fixed with cold methanol for 5 min at −20 °C, and permeabilized by quick washing with cold acetone. Cells were blocked by incubation with 10% FCS in PBS for 30 min at room temperature, followed by 1 h of incubation with the primary antibody. Cells were then incubated with the secondary antibody for 30 min. For fluorescence imaging, a Nikon Eclipse TE300 microscope equipped with a GFP filter (HQ FITC 41001) and Hamamatsu digital camera C4742-95 was used. A fluorescence filter was used to observe rhodamine (excitation 543 nm, mirror, emission 560 – 600 nm), Cy^{TM}5 (excitation 633 nm, dichroic 630 nm, emission 660 nm), and GFP (excitation 488, dichroic 560 nm, emission 505–525 nm). Confocal images were taken by a FV500 laser-scanning confocal microscope

[3] The abbreviations used are: MEMα, minimal essential medium α; EBSS, Earle's balanced salt solution; FCS, fetal calf serum; taxol, paclitaxel; Baf A, bafilomycin A1; GFP, green fluorescent protein; CHO, Chinese hamster ovary; PBS, phosphate-buffered saline.

equipped with a PLAPO 60 × 1.4 NA oil immersion lens and Fluoview software (Olympus). Movement of GFP-LC3 labeled autophagosomes was monitored using Olympus IX-70 confocal microscope with UPLAPO 40 × 0.85 NA. Cells were kept at 37 °C in 20 mM Tris, pH 7.4, in a micro-incubator (PDMI-2, Harvard Apparatus). All images were done at a rate of 1 frame every 10 s. Each experiment was performed at least five times, and representative images or movies of typical cells are depicted in the different figures.

For quantitative analysis of the formation of autophagosomes, cells expressing GFP-LC3 were incubated under normal growth or starvation conditions in the absence or presence of 0.1 μM Baf A. The number of autophagosomes per cell was determined by confocal microscopy at different times. The number of slices and their width were designed so that the entire cell was covered and that autophagosomes do not appear more than once. Each point represents the average ± S.D. obtained from ~60 cells. The counting was performed manually and validated by more than one person.

Electron Microscopy—Cells were grown on coverslips and fixed with 0.3% glutaraldehyde, 0.3% paraformaldehyde in cacodylate buffer (cacodylate 0.1 M, pH 7.4). The fixative was rinsed twice with cacodylate buffer, and samples were dyed in 1% OsO_4, 0.3% potassium dichromate, and 0.3% potassium ferrocyanide for 1–2 h followed by 1.5–2 h of incubation with 2% filtered uranyl acetate in H_2O. Ethanol was used for gradual dehydration of the samples and Epon for their embedding. To dissolve the glass coverslips, the Epon-embedded samples were incubated for 2 h in 20% hydrofluoric acid. Sections of 70–100 nm were viewed by transmission electron microscopy (Technai-12; Phillips, Eindhoven, The Netherlands).

Subcellular Fractionation—For cytosol and total membrane analysis, cells were grown in 100-mm diameter dishes, washed, and removed by a cell scraper. After resuspension in homogenization buffer (10 mM Tris, pH 7.4, 0.25 M sucrose, 1 mM phenylmethylsulfonyl fluoride, 0.5 μg/ml leupeptin, 2 μM pepstatin A, and 2 μg/ml aprotinin), cells were homogenized by Dounce homogenizer on ice. Unbroken cells and nuclei were removed by low speed centrifugation (3,000 rpm, 5 min), and the supernatant was centrifuged in TLA 100.2 (60,000 rpm, 30 min) for cytosol and total membrane fractions. Fractions were precipitated by 10% trichloroacetic acid and analyzed by Western blot. All immunoblots in this study are representatives of at least three experiments. For membrane flotation in the sucrose gradient, CHO cells were grown in suspension to ~0.5×10^6 cell/ml (3 liters), collected by centrifugation at low speed (2000 rpm for 6 min), resuspended in 4 pellet volumes of homogenization buffer, and homogenized as described previously (43). Unbroken cells were removed from the cell homogenate by centrifugation at 700 × *g* for 6 min. Cell homogenate was adjusted to 2 M sucrose and placed at the bottom of SW-28 tubes, followed by overlaying with layers of 1.75, 1.5, 1.25, 1, and 0.75 M sucrose. The gradients were centrifuged at 4 °C in SW-28 rotor (Beckman) at 25,000 rpm overnight with slow acceleration and deceleration. Fractions were collected continuously from the top of the gradient, and densities of the fractions were calculated from the refractive indices. From each fraction, 100-μl samples were precipitated by 10% trichloroacetic acid, and pellets were analyzed by Western blot.

Determination of Autophagosome Life Span—From the slope of the graphs obtained under control (Fig. 7*A*) conditions in the presence of Baf A, we calculated that the average time interval between successive autophagosome formation events is ~3.3 min. In the absence of Baf A, the average number of autophagosomes per cell remains constant and is equal to 9.8. Therefore, the autophagosome population is in a state of equilibrium (equal rates of autophagosome formation and degradation). Thus, successive degradation events also occur every 3.3 min, on average. The remaining information needed to calculate the autophagosome life span is the average number (hereby labeled X) of degradation events occurring between the formation of a given autophagosome and its degradation. A simple calculation shows that *X* is a geometric random variable whose average is 9.8 (44); that is, following the formation of a given autophagosome, 9.8 degradation events of other autophagosomes occur on average before our autophagosome is degraded. Thus, the average autophagosome life span under control conditions is 9.8 × 3.3 ≈32.7 min. Similarly, from the slope of the graph obtained under starvation conditions in the presence of Baf A (Fig. 7*B*), we infer that the average time interval between successive autophagosome formation events is 1.22 min. Therefore, when the autophagosome population reaches equilibrium, the time interval between successive degradation events is also ~1.22 min. From the graph in Fig. 7*B,* we deduced that under starvation conditions equilibrium is reached after 60 min with ~28 autophagosomes per cell. Then, as above, the average of *X* is 28, and the average life span of an autophagosome is ~28 × 1.22 ≈34.2 min. (As summarized in Table 1, these calculations were done as well under nocodazole treatment.)

Protease Protection Assay—Autophagic vacuole fractions were prepared by a sucrose gradient as described above. To concentrate the membranes, fractions were diluted with reaction buffer (Tris 10 mM, pH 7.4, 0.25 M sucrose), centrifuged at 90,000 rpm for 30 min, and pellets were resuspended in reaction buffer. For the protease protection assay, membranes were incubated at 37 °C for 30 min in a reaction buffer containing 10 μg/ml proteinase K (Sigma) in the presence or absence of 0.4% Triton X-100. Proteolysis was terminated by the addition of phenylmethylsulfonyl fluoride to a final concentration of 20 μM at 4 °C for 10 min. Samples were analyzed by immunoblotting using antibody against GFP.

Degradation of Long Lived Proteins—Degradation of long lived proteins was performed according to standard protocol (10). CHO cells stably expressing GFP-LC3 were grown to 70–80% confluence in 6-well plates (35 mm). Cells were then labeled for 14 h in medium containing [^{14}C]valine (0.5 μCi/ml) and 5% FCS in valine-free MEMα. After three rinses with PBS, cells were incubated in either valine-free MEMα or EBSS containing 0.1% bovine serum albumin and 10 mM cold valine. When required, 5, 15, or 25 μg/ml nocodazole, 100 nM wortmannin, 100 nM bafilomycin A, or 10 μM 3-methyladenine was added. After the 1-h incubation, the medium was replaced with identical fresh medium, and cells were incubated for additional 4 h. The medium was precipitated in 10% trichloroacetic acid, and trichloroacetic acid-soluble radioactivity was measured.

Total cell radioactivity was measured after lysis with 0.1 M NaOH. [^{14}C]Valine release was calculated as a percentage of the radioactivity in the trichloroacetic acid-soluble supernatant relative to the total cell radioactivity.

RESULTS

Lipidated GFP-LC3 Is Associated with Microtubules under Normal Growth and Starvation Conditions—To characterize the dynamics and intracellular route taken by autophagosomes in living cells, we established a CHO cell line that stably expresses GFP fused to the N terminus of LC3. The localization of GFP-LC3 in living cells was followed by confocal microscopy analysis. Under normal growth conditions (MEMα), most GFP-LC3 was found dispersed in the cytosol, although a significant fraction (resembling a mixture of vesicles and microtubule-like structures) was concentrated at the juxtanuclear region (Fig. 1*A*). When cells were transferred to a starvation medium (EBSS) to induce autophagy, GFP-LC3-labeled autophagosomes appeared in the cytoplasm within 30 min, peaking after about 1 h of incubation (Fig. 1*A*). These vesicles were also concentrated at the juxtanuclear region. In agreement with previous reports (10, 18), the change in cellular localization of LC3 was accompanied by the formation of LC3-II, the membrane-bound form of LC3 (Fig. 1*B*). Notably, the ratio of cytosol (supernatant) to membrane-bound (pellet) endogenous LC3 was similar to that found for GFP-LC3 (Fig. 1*B*). Previous studies showed that mutation of glycine at position 120 prevents the C-terminal cleavage and, consequentially, conjugation of LC3 to the autophagosomal membrane (19). Under normal growth conditions, GFP-LC3$_{G120A}$ was evenly distributed throughout the cell, unlike the juxtanuclear localization of GFP-LC3$_{wt}$ (see supplemental Fig. 1), indicating that the subcellular localization of GFP-LC3 is dependent on processing of its C-terminal region both under normal growth and starvation conditions.

To further characterize the change observed in GFP-LC3 localization, the profile of membranes associated with GFP-LC3 was determined in cell homogenates, separated by flotation on a sucrose density gradient (Fig. 1*C*). Wild-type GFP-LC3-I was obtained predominantly from the original loading fraction (Fig. 1*C*, *upper left panels, lane 1*), whereas only a small proportion of GFP-LC3-I was associated with dense fractions, containing endoplasmic reticulum membranes (Fig. 1*C*, *lanes 2* and *3*). Wild-type GFP-LC3 obtained from starved cells showed a dramatic shift in its fractionation profile. A large amount of the protein, consisting only of the lipidated form GFP-LC3-II, cofractionated with Golgi membranes in the light sucrose fractions (Fig. 1*C*, *lanes 4* and *5*). Consistently, the endogenous LC3-I and LC3-II, identified by specific anti-LC3 antibodies, were fractionated similarly to GFP-LC3 (data not shown). The fractionation profile of the mutant GFP-LC3$_{G120A}$ was similar to that of the wild-type GFP-LC3-I and did not change upon starvation (Fig. 1*C*, *right panels*).

We next examined the involvement of microtubules in the localization of GFP-LC3 under different growth conditions. To this end, cells expressing GFP-LC3 were grown in the presence (Fig. 2*A*) or absence (Fig. 2*B*) of amino acids, and microtubules were visualized with anti-α-tubulin antibodies. Under amino acid-rich conditions, GFP-LC3 was associated with the minus ends of microtubules, which were also immunostained by anti-γ-tubulin antibodies (Fig. 2*A*). To examine whether intact microtubules are essential for this localization, cells were pretreated with nocodazole, a microtubule-depolymerizing agent. Within 15 min of this treatment, tubulin became scattered uniformly in the cytoplasm (data not shown). As shown in Fig. 2*A* (and Fig. 2*D*), nocodazole induced a concomitant fragmentation of both microtubules and the juxtanuclear GFP-LC3 labeling, indicating that under normal growth conditions GFP-LC3 is concentrated toward the minus ends of microtubules in a microtubule-dependent manner.

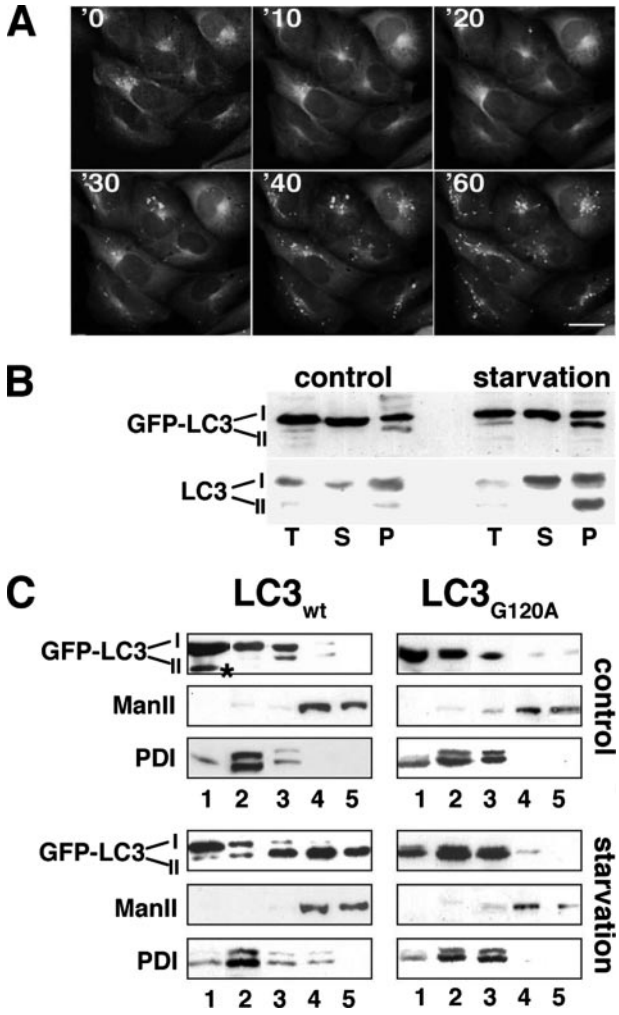

FIGURE 1. **GFP-LC3-II is associated with microtubules under normal and starvation conditions.** *A,* cells expressing GFP-LC3 were monitored by confocal microscopy under normal growth conditions (time 0 min) and at various time points following their transfer to EBSS (starvation) medium at 37 °C. *Scale bars*, 10 μm. *B,* Western blot of CHO cells stably expressing GFP-LC3. Cells were cultured for 2 h in 10% FCS/MEMα (*control*) or EBSS medium (*starvation*). Cell homogenate (*T*) (10% of the material used for further fractionations) was fractionated into the supernatant (*S*) and pellet (*P*) and immunoblotted using antibodies against LC3. LC3-I represents the unlipidated form, and LC3-II represents the lipidated form of the protein. GFP-LC3 was overexpressed in these cells to about 5–6-fold above the endogenous LC3 level. *C,* for subcellular fractionation analysis, cultured cell homogenates, obtained from wild-type GFP-LC3 (LC3$_{wt}$) and GFP-LC3$_{G120A}$ stably transfected cells, were floated on a sucrose density gradient as described under "Experimental Procedures." Fractions were precipitated and analyzed by immunoblotting using anti-GFP, anti-ManII (for Golgi), or anti-protein disulfide (*PDI*) (for endoplasmic reticulum) antibodies. *Lanes 1–5* show fractions of 53, 45, 37, 32, and 28% sucrose, respectively. *Asterisk* represents a nonspecific band.

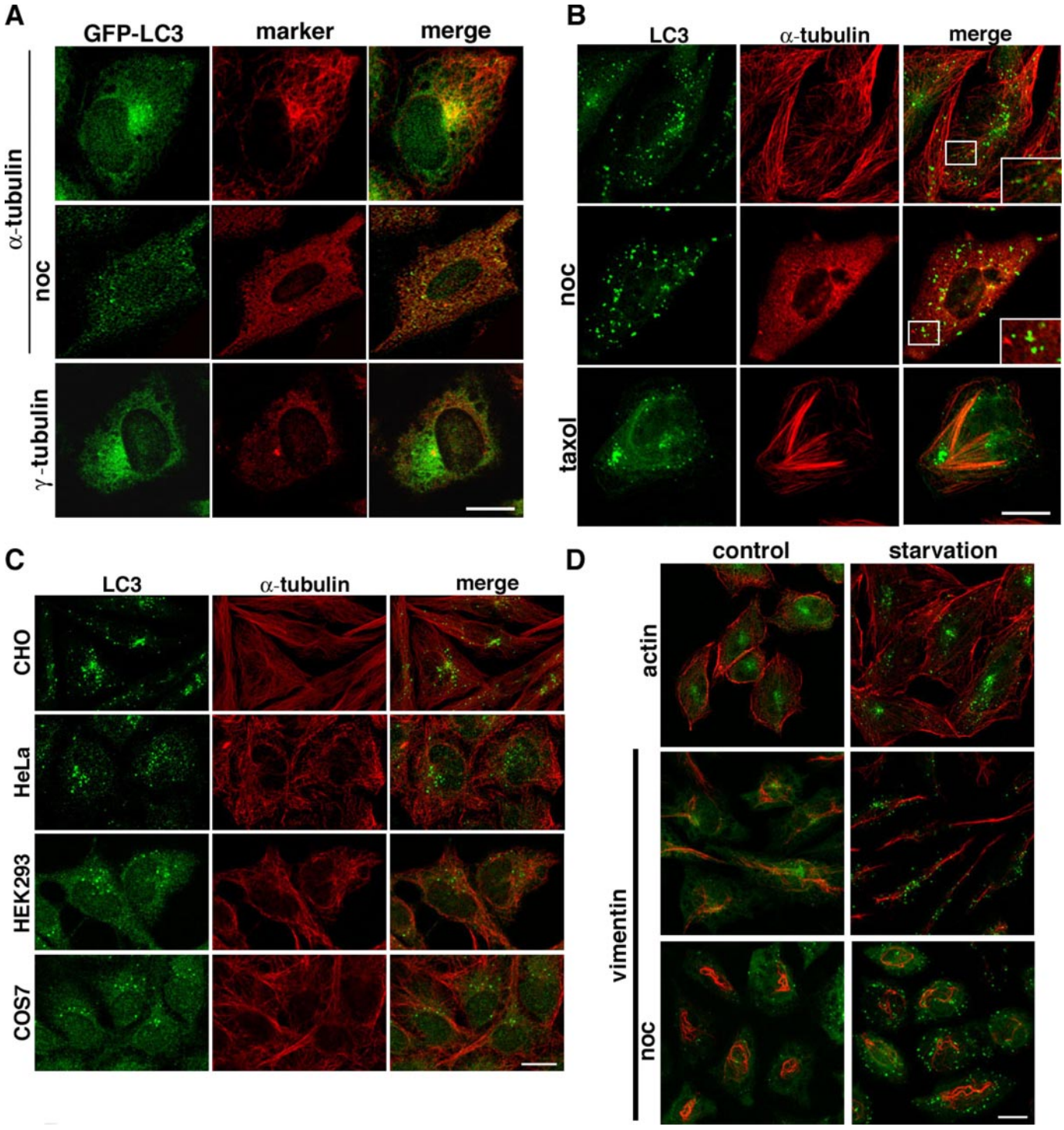

FIGURE 2. **Autophagosomes are associated with the microtubule network.** *A,* CHO cells expressing GFP-LC3 were incubated in the presence or absence of 5 μg/ml nocodazole (*noc*), and microtubules or microtubule organizing center were immunostained by monoclonal anti-α-tubulin or anti-γ-tubulin antibodies, respectively. *B,* cells expressing GFP-LC3 were incubated under starvation conditions for 2 h in the absence or presence of nocodazole or taxol and subjected to immunofluorescence confocal microscopy using anti-α-tubulin antibodies. *C,* CHO, HeLa, HEK-293, and COS7 cells were incubated under starvation conditions for 2 h and then fixed and stained for endogenous LC3 and microtubules using anti-LC3 or anti-α-tubulin antibodies, respectively. *D,* cells expressing GFP-LC3 were starved for 2 h in the absence or presence of nocodazole and immunostained for intermediate and microfilaments using anti-vimentin and anti-actin antibodies, respectively. *Scale bars,* 10 μm.

We next analyzed the localization of LC3 under amino acid deprivation (Fig. 2*B*). Under these conditions, GFP-LC3-labeled autophagosomes concentrated around the microtubule organizing center and appeared adjacent to microtubules. When cells pretreated with nocodazole were transferred to starvation medium (also containing this drug), the GFP-LC3-labeled autophagosomes were distributed throughout the cytoplasm with no evidence for juxtanuclear localization (Fig. 2*B*). Taxol, a drug that prevents depolymerization of spindle fiber microtubules, shifted the localization of autophagosomes to the

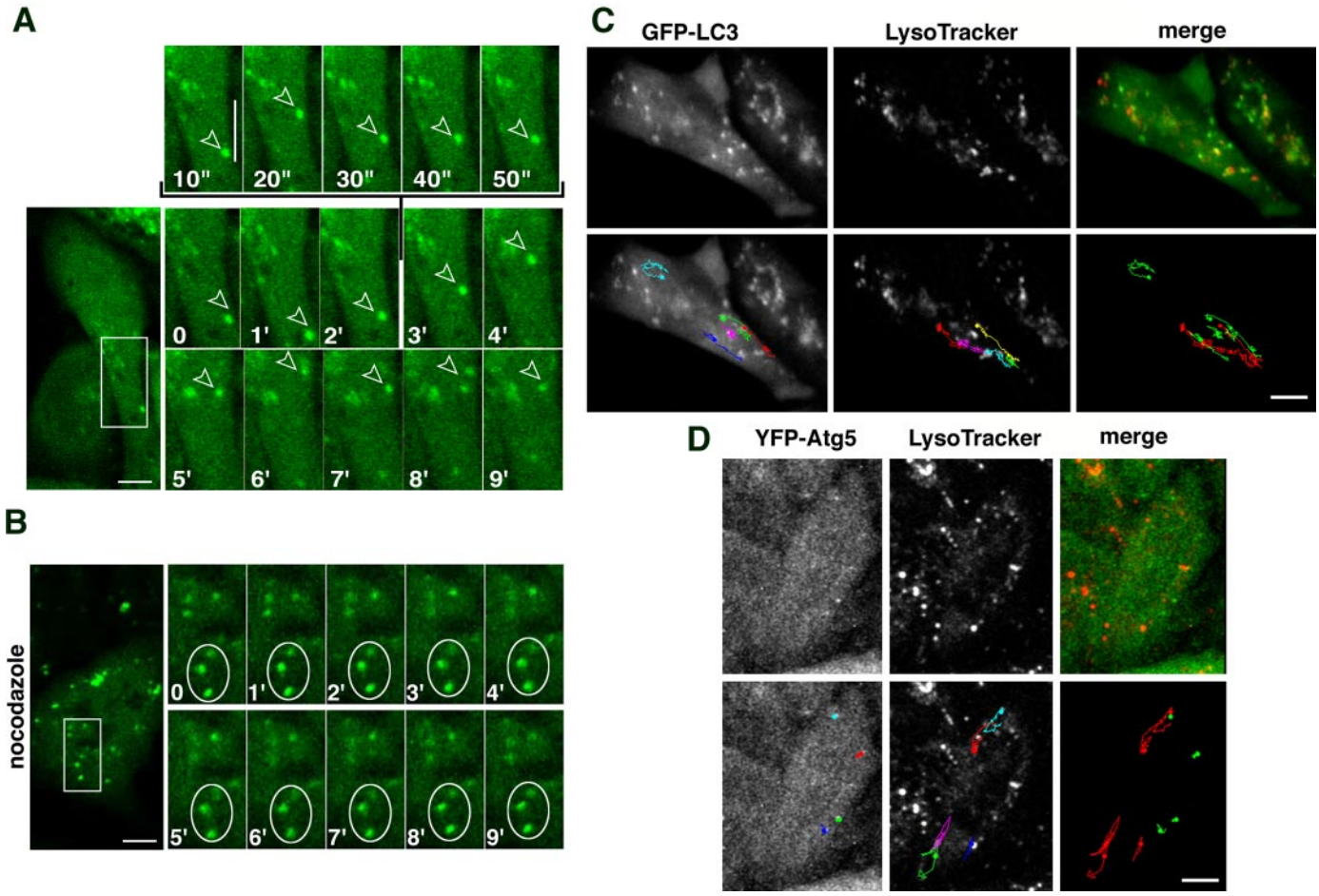

FIGURE 3. **Mature autophagosomes are microtubule-dependent dynamic organelles.** Movement of autophagosomes in starved cells was followed by real time video microscopy. Cells were incubated in starvation medium at 37 °C in the absence (*A*) or presence (*B*) of nocodazole (5 μg/ml) and frames were recorded every 10 s. The *boxed area* on the *left frame* of *A* and *B* was enlarged, and *frames* (on the *right*) show time-lapse images of 1-min intervals during a 9-min period. Frames of *upper panels* (*A*) show time-lapse images of 10-s intervals between a 2- and 3-min period. Tracking analysis represents a 10-min period of movement of single GFP-LC3-labeled autophagosomes and LysoTracker-labeled lysosomes (*C*) or YFP-Atg5 labeled structures and LysoTracker-labeled lysosomes (*D*). Tracks for individual vesicles on the *left panels* were marked in different colors, and on the *right* (*merge panel*), lysosomes were marked *red* and autophagosomes or phagophores *green*. *Scale bars*, 5 μm.

microtubule poles (Fig. 2*B*), further supporting the association of these organelles with microtubules. This association was limited not only to GFP-LC3 expressed in CHO cells. By utilizing anti-LC3 antibodies, we examined the localization of endogenous LC3-labeled autophagosomes in cell lines other than CHO, including HeLa, HEK-293, COS-7 (Fig. 2*C*), as well as PC12 and human melanoma cells (Fig. 8*C*). In all of these cell types, LC3 exhibited a similar microtubule-dependent juxtanuclear localization of autophagosomes, which was further confirmed by double labeling with anti-γ-tubulin antibodies (data not shown). No association of LC3-labeled autophagosomes with other cytoskeletal filaments such as intermediate or microfilaments was observed (Fig. 2*D*). Taken together, these results demonstrate that LC3-labeled autophagosomes are associated with the microtubule network in various cell types.

Autophagosomes, but Not Phagophores, Are Microtubule-dependent Dynamic Organelles—Given that microtubules and associated molecular motors are responsible for intracellular movement of organelles and vesicles, we tested whether autophagosomes also move along these tracks. We followed autophagosome dynamics in cells expressing GFP-LC3 by time-lapse video microscopy at 10-s intervals for a 10-min period (Fig. 3). Autophagosomes appeared as highly dynamic organelles exhibiting rapid movements. Analysis of a typical autophagosome revealed long distance, rapid directional movements of about 3 μm/10-s period, followed by short, random movements or pauses (Fig. 3*A*, *arrowhead*; for movie see supplemental video 1). The rapid, long distance directional movements were observed in both centrifugal and centripetal directions between the cell equator and the periphery, suggesting progression along microtubules. Indeed, application of nocodazole invariably abolished this type of movement (Fig. 3*B*) indicating that autophagosome movement is microtubule-dependent. Further analysis of this movement revealed that autophagosomes tend to move along distinct tracks similar to LysoTracker-labeled lysosomes (Fig. 3*C* and supplemental video 2). The rapid movements of both lysosomes and autophagosomes were totally abolished by nocodazole (for a movie see supplemental video 3), taxol, and by reducing temperature to 16 °C (data not shown).

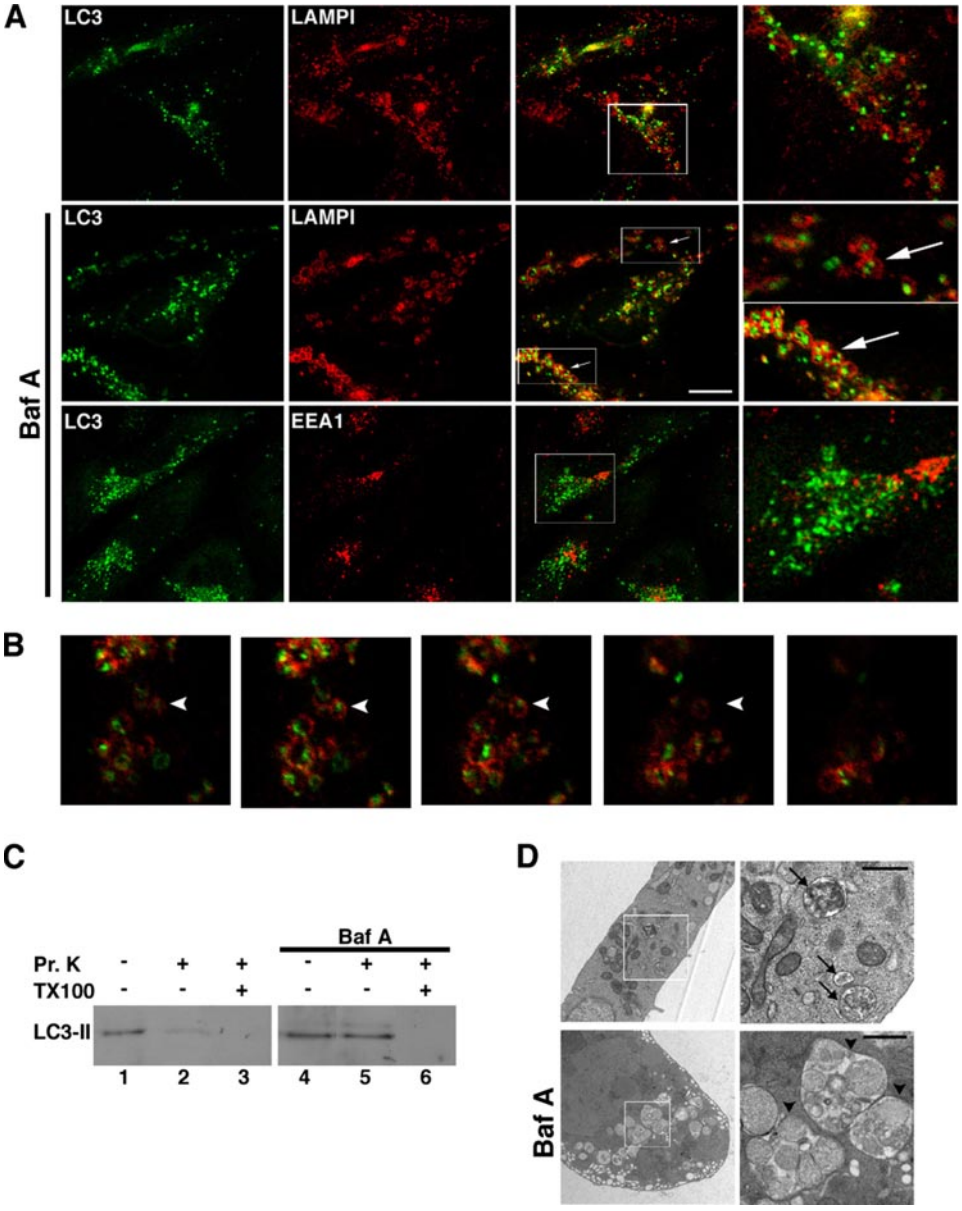

FIGURE 4. **Formation of autolysosomes is stabilized under Baf A treatment.** *A,* cells expressing GFP-LC3 were incubated under starvation conditions in the absence or presence of 0.1 μM Baf A for 2 h. Lysosomes or early endosomes were labeled with monoclonal antibodies against LAMPI or EEA1, respectively, and colocalization was analyzed by confocal microscopy. *Arrows* depict autolysosomes (GFP-LC3-labeled membranes within lysosomes). *Scale bar,* 10 μm. *B,* sequential confocal sections (slices of 0.25 μm) of autolysosomes. *C,* protease protection assay. GFP-LC3 expressing cells were starved in the absence (*lanes 1–3*) or presence of Baf A (*lanes 4–6*). Autophagosomes fractions (for details see "Experimental Procedures") obtained from these cells were incubated at 37 °C for 30 min in the absence (*lanes 1* and *4*) or presence (*lanes 2, 3, 5,* and *6*) of proteinase K (*Pr. K*). In *lanes 5* and *6*, 0.4% Triton X-100 (*TX100*) was added. Samples were subjected to immunoblotting with antibodies against LC3. *D,* CHO cells were incubated under starvation conditions in the absence or presence of 0.1 μM Baf A for 2 h, fixed, and analyzed using electron microscopy. *Arrows* show the empty lysosomes, and the *arrowheads* show the accumulation of autophagic bodies within autolysosomes in Baf A treatment. *Scale bar,* 0.5 μm.

Previous studies demonstrated that both Atg5 and LC3 are associated with the phagophore membrane (also known as the isolation membrane) at the site of autophagosome formation, but only LC3 remains associated with mature autophagosomes (10). To determine whether phagophores also move along microtubules, YFP-Atg5 was stably expressed in CHO cells and followed by time-lapse video microscopy. We confirmed that in this experimental system, YFP-Atg5-labeled vesicles were detected only after amino acid deprivation and were colabeled with anti-Atg16 or anti-LC3 antibodies, indicating that these dots represent *bona fide* phagophores (data not shown). As shown in the time-lapse tracking analysis obtained from a 10-min period, YFP-Atg5-labeled structures were immobile, unlike the LysoTracker-labeled lysosomes (Fig. 3*D* and supplemental video 4). We conclude that mature autophagosomes move along microtubules, whereas phagophores remain immobile.

Autolysosomes Are Formed in the Presence or Absence of Intact Microtubules—Among its other functions, the microtubule network is being utilized for organizing vesicular transport. To determine whether microtubules are required for targeting and fusion of autophagosomes with lysosomes, we first set up conditions for detecting the product of this transport step, namely autolysosomes. As these organelles are short lived and are rarely detected, inhibition of the lysosomal catabolic activity is essential to stabilize and visualize them. Accordingly, the dynamics of autophagosome formation and degradation were characterized by starving cells in the presence or absence of the vacuolar H^+-ATPase inhibitor bafilomycin A (Baf A). Inhibition of lysosomal acidification by Baf A (31) or chloroquine (32) is known to block activity of the pH-dependent lysosomal proteases and is thus expected to bring about accumulation of autolysosomes. It has been reported that Baf A inhibits autophagy, with production of autolysosomes (31). However, other reports have suggested that Baf A inhibits fusion between autophagosomes and lysosomes, *i.e.* formation of autolysosomes (33). To directly address this issue, we labeled lysosomes of the stably transfected GFP-LC3 starved cells with anti-LAMPI antibodies. As depicted in Fig. 4*A*, only a small fraction of lysosomes and autophagosomes colocalized in the absence of Baf A. However, in the presence of Baf A most LC3-labeled membranes were found within lysosomes (Fig. 4*A*; see also Fig. 5*B*), whereas no colocalization was detected with the early endosome marker EEA1. Under these conditions, the LAMPI-labeled membranes appeared enlarged and in many cases contained more than one autophagic body. Quantification of these enlarged lysosomes

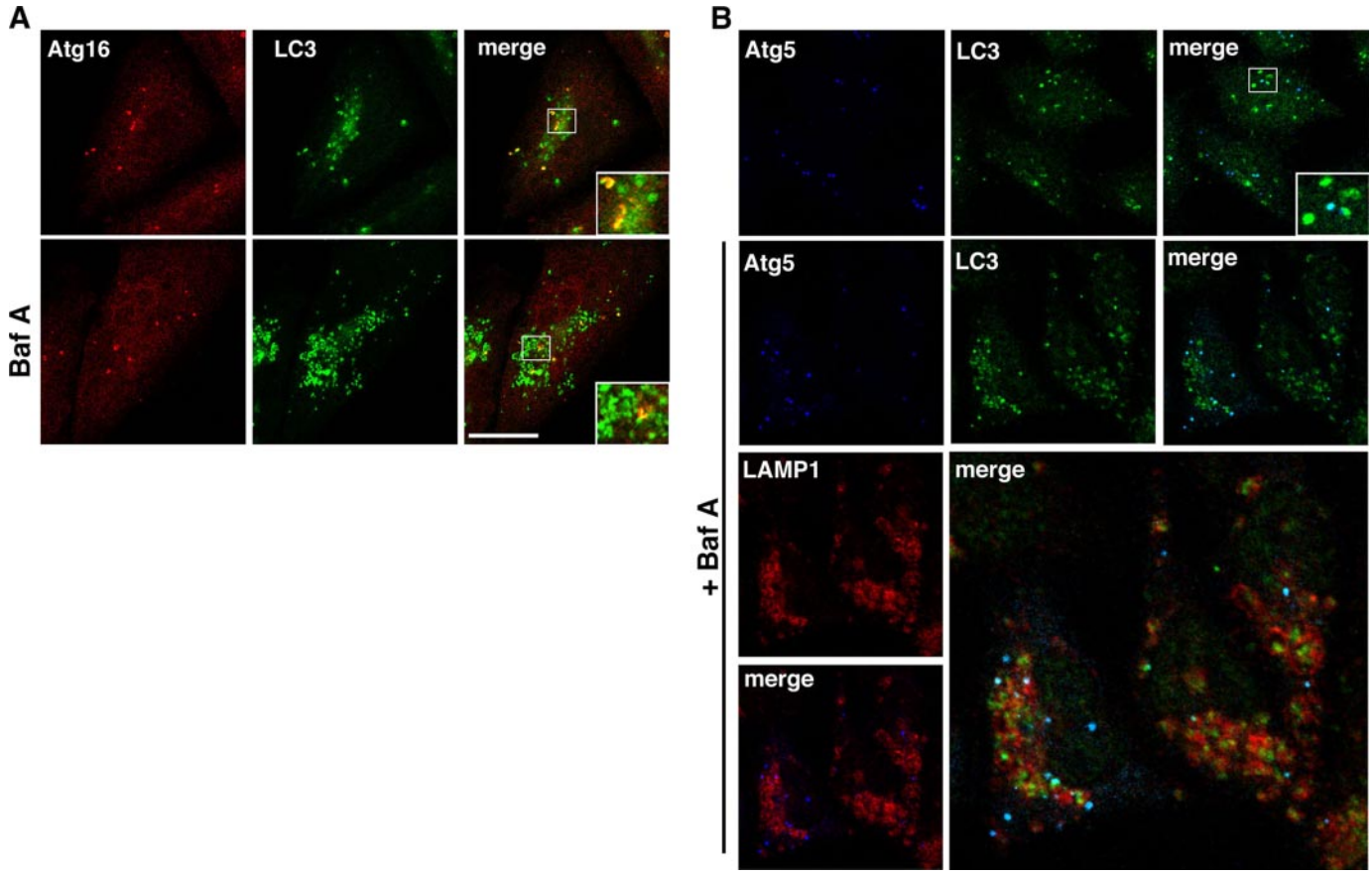

FIGURE 5. **The level of LC3/Atg5/Atg16-labeled structures under starvation following Baf A treatment.** CHO cells were incubated for 2 h under starvation conditions in the absence or presence of 0.1 μM Baf A. Cells stably expressing either GFP-LC3 (*A*) or YFP-Atg5 (*B*) were stained by polyclonal antibodies against Atg16 (*A*) or LC3 and LAMPI (*B*), respectively. *Scale bar*, 10 μm.

showed an average increase of ~30% in diameter (~1.2 μm) compared with normal conditions (~0.9 μm). A sequential Z-section (0.2 μm) analysis was performed to ensure that GFP-LC3 was indeed localized within lysosomes (Fig. 4*B*).

Our results suggest that Baf A blocks lysosomal degradation without affecting autophagosome-lysosome fusion. To verify the topology of LC3-II biochemically, we performed a protease protection assay of membranes purified from control and Baf A-treated cells. Although LC3-II from cells grown in the absence of Baf A was mostly degraded by proteinase K (Fig. 4*C, lane 2*), LC3-II from Baf A-treated cells was protected from proteolysis (Fig. 4*C, lane 5*), indicating that Baf A treatment leads to the accumulation of LC3-II within enclosed membranes. Consistently, transmission electron microscopy analysis demonstrated that treatment with Baf A resulted in swollen lysosomes containing a large number of nondegraded autophagic bodies (Fig. 4*D*).

Inhibition of lysosomal proteolysis by Baf A did not affect early steps of autophagosome formation, because the level of phagophores labeled by Atg5/Atg16 under starvation conditions did not change in the presence of Baf A, although that of vesicles labeled by GFP-LC3 or endogenous LC3 was significantly elevated (Fig. 5, *A* and *B*). Note that although vesicles labeled with LC3 alone accumulated within lysosomes under Baf A treatment, phagophores labeled by LC3 and YFP-Atg5 were excluded from lysosomes (Fig. 5*B*). Taken together, our findings show that Baf A treatment does not inhibit the fusion of autophagosomes with lysosomes but rather inhibits lysosomal degradation, thus leading to the accumulation of autophagic bodies within lysosomes.

To examine whether microtubules are essential for delivery and fusion of autophagosomes with lysosomes, CHO cells expressing GFP-LC3 were pretreated with nocodazole and then starved in the presence or absence of Baf A. As in the case of intact microtubules, Baf A treatment resulted in a dramatic accumulation of LC3-labeled vesicles, found mostly within LAMP1-labeled lysosomes (Fig. 6*A*). Furthermore, transmission electron microscopy analysis of these cells clearly demonstrated the accumulation of autophagic bodies within lysosomes (Fig. 6*B*). These findings demonstrate that intact microtubules are not required for autophagosome-lysosome fusion. Recently, Kochl *et al.* (27) have reported that nocodazole treatment of primary hepatocytes reduced the extent of colocalization between lysosomes (LysoTracker) and autophagosomes (GFP-LC3), suggesting a role of microtubules in their fusion process. To further examine whether microtubule disassembly affects fusion between lysosomes and autophagosomes, we quantified the number of GFP-LC3-labeled vesicles interior and exterior to lysosomes in cells treated with Baf A in the absence or presence of nocodazole. As depicted in Fig. 6*C*, the percentage of GFP-LC3 labeled vesicles within lysosomes (autophagic bodies) was not altered by nocodazole treatment,

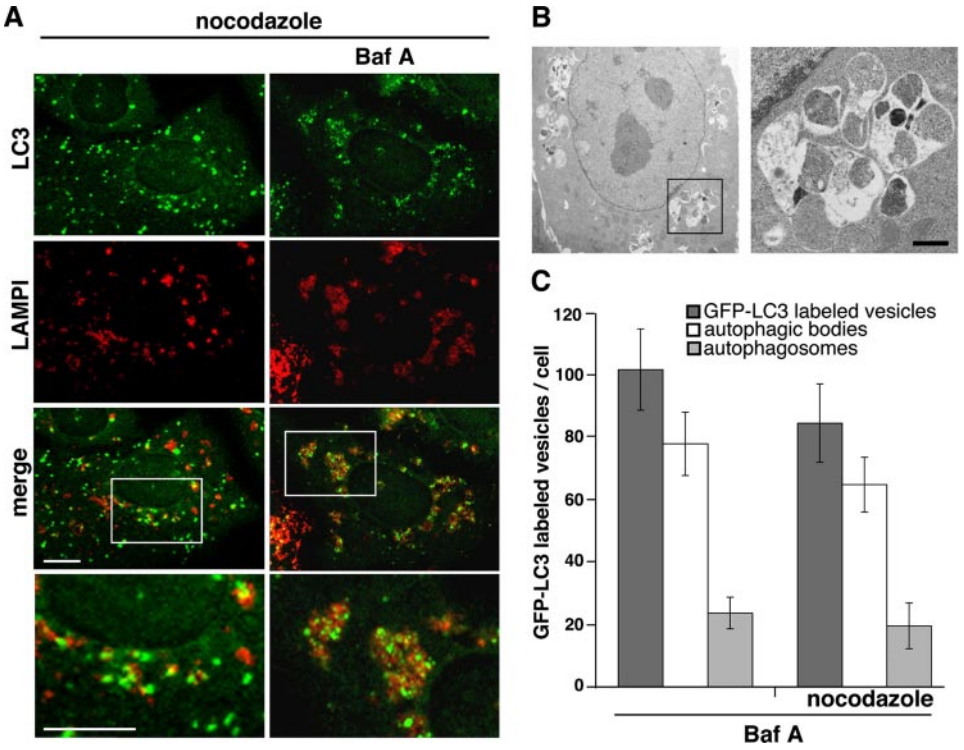

FIGURE 6. **Intact microtubules are not essential for fusion of autophagosomes with lysosomes.** *A,* CHO cells expressing GFP-LC3 were starved for 2 h in the presence of nocodazole or nocodazole and Baf A. Lysosomes were labeled with monoclonal antibodies against LAMPI, and colocalization of autophagosomes and lysosomes was analyzed by confocal microscopy. *White boxes* are enlarged to show the level of colocalization. *Scale bar*, 5 μm. *B,* cells were incubated for 2 h under starvation conditions in the presence of 0.1 μM Baf A and 5 μg/ml nocodazole, fixed, and analyzed using electron microscopy. *Scale bar,* 0.5 μm. *C,* Baf A-treated cells were starved for 2 h in the absence or presence of nocodazole, and lysosomes were stained with LAMPI antibodies. The number of GFP-LC3-labeled autophagic bodies and autophagosomes per cell was determined by confocal microscopy and represents the average ± S.D.

indicating that in our system microtubule depolymerization does not affect the rate of autolysosome formation.

Microtubule Disassembly Affects Autophagosomes Formation but Not Their Life Span—As shown above, targeting and fusion of autophagosomes with lysosomes can take place in the absence of intact microtubules. In other trafficking pathways, such as delivery of vesicles to the plasma membrane, microtubules were suggested to act as traffic facilitators. Therefore, we quantified the level and kinetics of autophagy in the presence or absence of microtubule poisons. The average number of GFP-LC3-labeled vesicles per cell was determined under different growth conditions. As the number of autophagosomes per cell is determined by the rate of their formation *versus* degradation, blocking lysosomal degradation by Baf A, thereby inhibiting autophagosome degradation without affecting their formation (see Fig. 5), reveals the overall rate of autophagosome formation. As depicted in Fig. 7*A* (and Table 1), under control conditions the number of GFP-LC3-labeled vesicles at steady state is ~10 autophagosomes per cell, and their formation rate is 0.3 autophagosomes per min. Under starvation conditions (Fig. 7*B*), the number of vesicles increased gradually, reaching a steady state level of about 30 vesicles per cell with formation rate of ~0.8 autophagosomes per min. Nocodazole treatment showed a significant decrease (~25%) of autophagosome formation rate (Fig. 7, *A* and *B*, Table 1, and Fig. 6*C*), leading to an overall reduced number of autophagosomes (also ~25%) at steady state.

Next, by using the data presented above (Fig. 7, *A* and *B*), we determined whether microtubule depolymerization affects the life span of autophagosomes. As autophagosomes are highly dynamic organelles, determination of their kinetic parameters by direct video microscopy may turn misleading. In addition, the often occurring collisions between individual autophagosomes, as well as between autophagosomes and lysosomes (see supplemental video 4 and supplemental Fig. 2), bring another factor of uncertainty to their tracking. Moreover, in many cases the disappearance and appearance of these vesicles may be accounted for by their vertical movement in and out of the focus plane. To overcome these difficulties, we utilized a mathematical approach to calculate autophagosome life span using fixed cells. Two parameters (deduced from the graphs in Fig. 7, *A* and *B*, and summarized in Table 1) are required to calculate the autophagosome average life span as follows: the average number of autophagosomes per cell at steady state and the rate of their formation. Simply multiplying these two parameters gives the average life span of the autophagosomes (see elaborated explanation under "Experimental Procedures"). As summarized in Table 1, the life span of an autophagosome resides between 30 and 35 min and was not affected by microtubule disruption. Consistent with our calculation, direct monitoring of single autophagosomes, carried out at areas where distinct autophagosomes and lysosomes could be detected, showed that the time duration between appearance and disappearance of a given GFP-LC3-labeled vesicle was indeed 30–40 min (Fig. 7*C*). Notably, the disappearance of LC3-labeled autophagosomes was associated with colocalization with lysosomes labeled with LysoTracker (Fig. 7*C*). In summary, we show that microtubule depolymerization affects the rate of autophagosome formation but not their life span. Hence, the data presented here further indicate that intact microtubules are not essential for the fusion event, implying that targeting of autophagosomes to lysosomes may not be the rate-limiting step in this pathway.

An alternative approach to study the dynamics of the autophagic process is by determining the rate of autophagosome disappearance under conditions where amino acids are added to the growing medium. To this end, cells expressing GFP-LC3 were starved for 2 h to induce autophagosome formation and then allowed to recover in amino acid-rich medium (MEMα) for different times. As shown in Fig. 8*A*, most autophagosomes disappeared within 30–45 min. These values further support the life span calculations presented above. As depicted in Fig. 8*B*, microtubule disassembly by nocodazole had no effect on

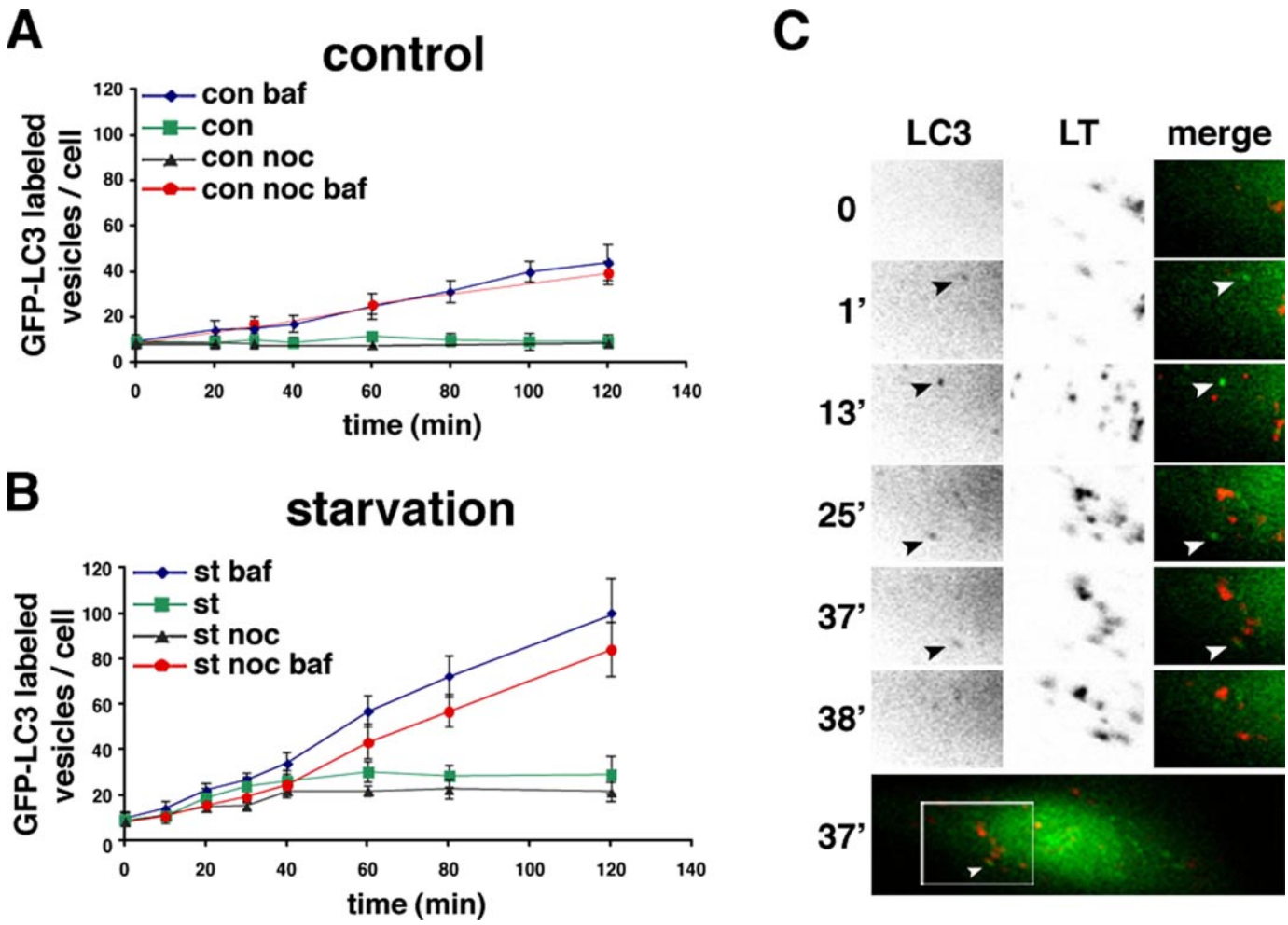

FIGURE 7. **Determining the rate of autophagosome formation and degradation under different conditions.** Cells expressing GFP-LC3 were incubated under control (*A*) or starvation (*B*) conditions in the absence or presence of 0.1 μM Baf A. The number of autophagosomes per cell was determined by confocal microscopy at different times. Each point represents the average ± S.D. obtained from ~60 cells. *C*, video microscopy monitoring directly the life span of a GFP-LC3-labeled autophagosome in cells incubated in starvation medium at 37 °C with lysosomes/late endosomes labeled by LysoTracker (*LT*).

TABLE 1

Rate of formation and average life span of autophagosomes under different growth conditions

The abbreviations used are as follows: aut, autophagosomes; con, control; st, starvation; noc, nocodazole.

Treatment	Aut/cell at steady state	Formation rate	Life span
		aut/min	*min*
Con	9.8 ± 3.2	0.30	32.3
Con + noc	8.1 ± 3.3	0.26	31.6
st	28.5 ± 3.5[a]	0.82	34.8
st + noc	21.6 ± 5.8[a]	0.66	32.8

[a] $p < 0.005$.

the ability of cells to degrade existing autophagosomes following transfer to MEMα.

Alternatively, we have tested the ability of pre-existing autophagosomes to be delivered for lysosomal degradation by utilizing the phosphatidylinositol 3-kinase inhibitor wortmannin, known to inhibit formation of new autophagosomes (34–36). Hence, treatment of starved cells with this drug again resulted in an overall reduction in the autophagosome level, in a similar time frame, regardless of nocodazole treatment (Fig. 8*B*). In all treatments, the level of GFP-LC3-II in the membrane fraction (pellet) was correlated with the appearance of autophagosomes (Fig. 8*B*, Western blot at the bottom of each panel). This phenomenon was observed in various cell lines (Fig. 8*C*). Taken together, these results indicate that microtubule disruption reduces autophagosome formation without affecting the normal duration of autophagy.

Microtubule Disruption Delays the Transport of Proteolytic Enzymes to Lysosomes—Our results indicate that microtubule depolymerization inhibits autophagosome formation by up to 25%. Previous reports indicated that microtubule disassembly induced by toxins such as nocodazole and vinblastine dramatically inhibits autophagy-mediated protein degradation (27, 30). To further characterize the role of microtubules in our system, we tested the effect of nocodazole on autophagy-mediated protein degradation. To this end, CHO cells were prelabeled with [^{14}C]valine for 16 h, and protein degradation was monitored after cells were transferred to starvation medium for 4 h. As depicted in Fig. 9*A*, this treatment resulted in about 50% increase in protein degradation activity, which, in turn, was inhibited in the presence of wortmannin, 3-methyladenine, or Baf A. Applying nocodazole at concentrations sufficient to depolymerize microtubule network and immobilize autophagosomes and lysosomes (5 μg/ml) reduced protein degradation

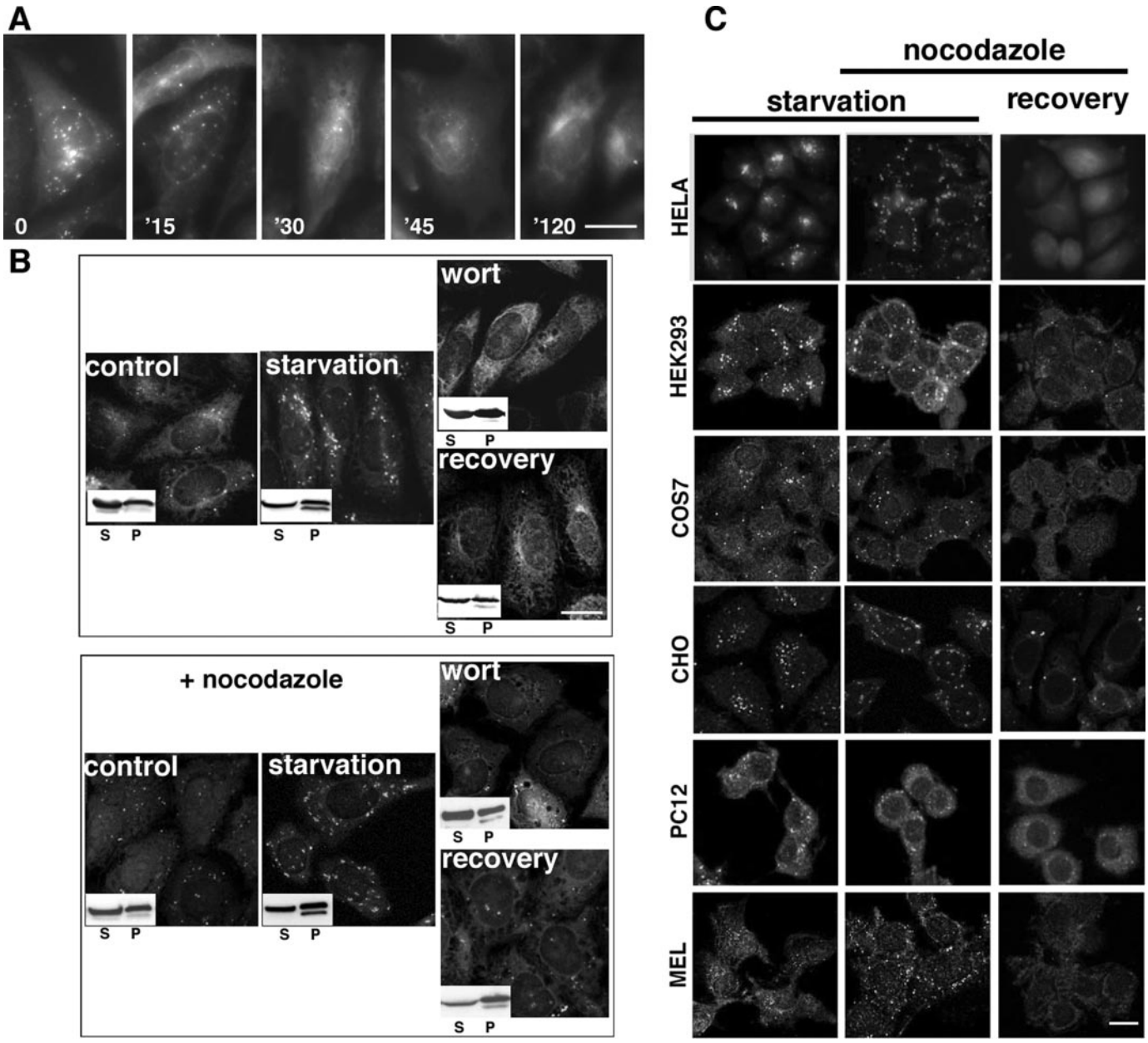

FIGURE 8. **Recovery from starvation does not require intact microtubule network.** *A,* CHO cells expressing GFP-LC3 were starved for 2 h (time 0) and allowed to recover in amino acid-rich medium (MEMα) for different times. *B,* cells were incubated for 2 h in the absence or presence of nocodazole in MEMα (*control*) and EBSS medium (*starvation*). Next, starved cells were transferred to MEMα for 40 min recovery in the absence or presence of nocodazole. Alternatively, starved cells were further incubated in EBSS medium for 40 min in the presence of wortmannin (*wort*) (0.1 μM). For immunoblotting analysis, cells were homogenized as described under "Experimental Procedures," and soluble and membrane-associated GFP-LC3 was detected by anti-GFP antibodies. *S,* supernatant; *P,* pellet. *Scale bar,* 10 μm. *C,* HeLa, HEK-293, COS-7, CHO, PC12, and human melanoma (*MEL*) cells were incubated for 2 h in the absence or presence of nocodazole. Cells starved in the presence of nocodazole were transferred to MEMα for a 40-min recovery in the presence of nocodazole as well. Cells were stained for endogenous LC3 using anti-LC3 antibodies.

by 20–25% (Fig. 9*A*). When higher concentrations of nocodazole were used (15 and 25 μg/ml), degradation was inhibited in a dose-dependent manner, corroborating previous reports (27, 30) (Fig. 9*A*). Based on these results, we propose that the direct effect of microtubule disruption is on autophagosome formation; the observed inhibition in protein degradation at high drug concentrations is not directly related to the targeting and fusion processes. In fact, when starved cells were treated with nocodazole for extended times (7 h), LC3 accumulated within lysosomes, suggesting that lysosomal activity is inhibited under these conditions (Fig. 9*B*). Also, under these conditions the lysosomal protease cathepsin D-GFP was excluded from the lysosomes (Fig. 9*C*), indicating that the delivery of lysosomal factors into the lysosome was defected under these conditions.

DISCUSSION

Autophagy represents a unique intracellular trafficking pathway whereby external signals, such as amino acid deprivation, lead to the production of new organelles, termed autophagosomes that are delivered for degradation in lysosomes/vacuoles. The whole process may be divided into several defined stages as follows: formation of phagophores, formation of mature auto-

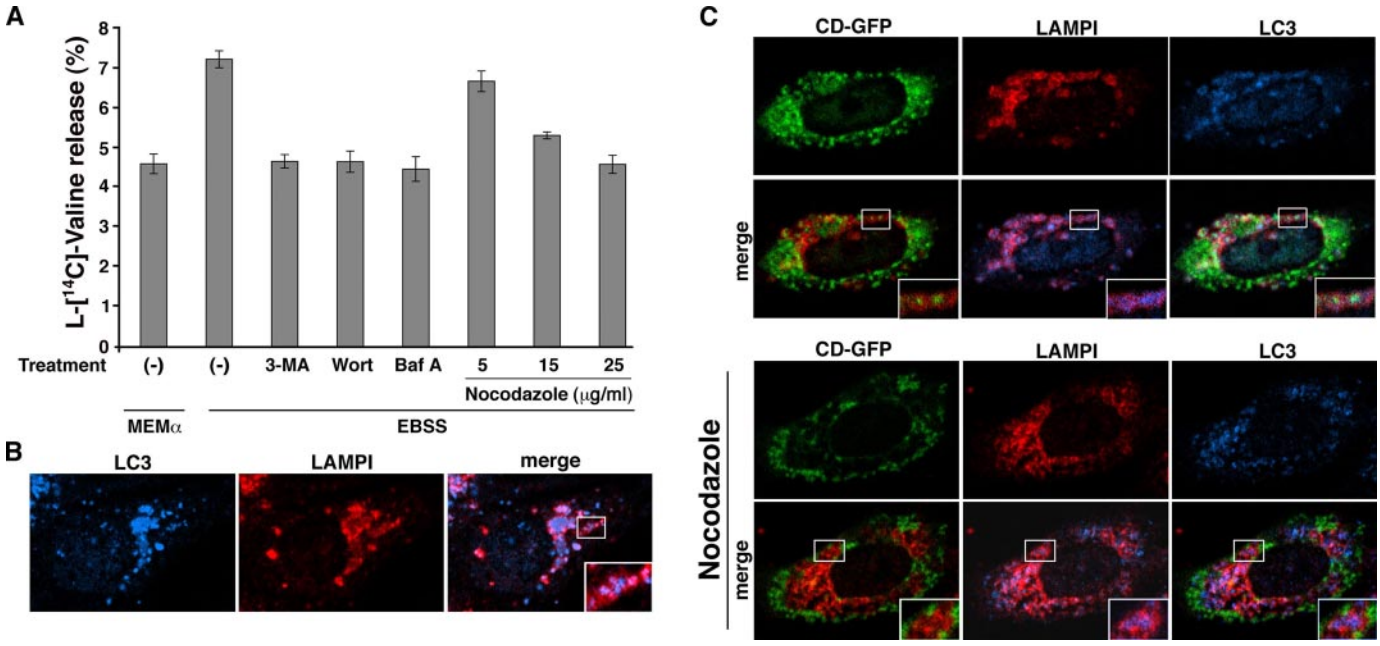

FIGURE 9. **Long periods of microtubule disruption inhibit the lysosomal proteolytic activity.** *A,* following the procedures described under "Experimental Procedures," the rate of degradation of long lived proteins was measured in CHO cells incubated in either MEMα or EBSS medium in the absence or presence of 3-methyladenine (*3-MA*) (10 μM), wortmannin (0.1 μM), nocodazole (5, 15, and 25 μg/ml), or Baf A (0.1 μM). Values express the percentage of cellular proteins degraded in 4 h represented as the means $\pm$ S.D. of nine determinations. *B,* CHO cells were starved for 7 h in the presence of 5 μg/ml nocodazole. Autophagosomes and lysosomes were labeled using antibodies against LC3 (*blue*) or LAMP1 (*red*), respectively. *C,* CHO cells expressing cathepsin D-GFP (*CD-GFP*) were incubated under starvation conditions in the presence of 0.1 μM Baf A and in the absence or presence of 5 μg/ml nocodazole. Lysosomes and autophagosomes were labeled using antibodies against LAMP1 (*red*) or LC3 (*blue*), respectively, and colocalization was analyzed by confocal microscopy. Areas in the *white boxes* are enlarged on the *left corner*.

phagosomes, targeting and trafficking of autophagosomes to lysosomes, formation of autolysosomes by fusion between autophagosomes and lysosomes, and, finally degradation of the autophagic bodies within the lysosomes. In this study we combined multiple experimental approaches to determine the involvement of the microtubule network in each step along the autophagic pathway. We show that only mature autophagosomes are associated and move along microtubules en route to lysosomes. Our results indicate that in the absence of intact microtubules autophagosomes are formed but at a significantly lower rate. However, targeting and fusion of autophagosomes with lysosomes are not affected by microtubule disassembly. Based on these findings we propose that microtubules facilitate autophagosome formation and may act as a barrier between phagophores and autophagosomes.

In most trafficking systems, microtubules facilitate the delivery of vesicles to their final long distance targets (37). Here we show that autophagosomes utilize microtubule tracks on their way to lysosomes. However, disruption of microtubules does not affect the kinetics of the trafficking step. The data presented are consistent with the hypothesis that targeting of autophagosomes to lysosomes may not be the rate-limiting step in this pathway. In our real time video experiments, we noticed that moving autophagosomes and lysosomes often associate with each other; however, in most cases, they dissociate without fusion (see supplemental Fig. 2 and supplemental video 2). Moreover, we found that when autophagy is induced in the absence of intact microtubules, autophagosomes are found at the vicinity of lysosomes (see Fig. 6*A* and supplemental video 3), thus reducing the need for large distance movements. If targeting of autophagosomes to lysosomes was a rate-limiting step, the overall life span of autophagosomes would be reduced under these conditions. We detected, however, no difference in the average autophagosome life span in the presence or absence of intact microtubules, indicating that the rate-limiting step(s) is downstream of the targeting process, namely tethering and/or fusion with the lysosomal membrane. We have recently found that the *N*-ethylmaleimide-sensitive factor ATPase activity, the major intracellular fusion factor that participates in the fusion between autophagosomes and lysosomes (38), is attenuated when autophagy is induced (39), thus providing a possible explanation for the slow autophagosome-lysosome membrane fusion.

Treatment of cells with Baf A results in the accumulation of autophagic vesicles and inhibition of autophagy-mediated protein degradation. Two previous reports disagree on the issue as to which step in the autophagic process is inhibited by this treatment. Based mainly on electron microscopy analysis, Yamamoto *et al.* (33) suggest that Baf A inhibits the fusion between the autophagosomes and lysosomes. However, by combining electron microscopy and biochemical analysis, Mousavi *et al.* (31) concluded that Baf A had no inhibitory effect on fusion but rather on intra-lysosomal degradation. Here we examined this question by utilizing biochemical, morphological, and immunohistological approaches, all of which indicate that Baf A has no effect on fusion of autophagosomes with lysosomes but, rather, it inhibits degradation within the lysosome. We argue that by blocking the vacuolar H^+-ATPase localized on lysosomes, Baf A inhibits lysosomal acidification leading to the accumulation of autophagic bodies within lysosomes. This

treatment allows the detection of GFP-LC3 within autolysosomes, thus providing a suitable experimental tool to study fusion between autophagosomes and lysosomes in living cells.

Among their other functions, microtubules serve as roadways for membrane traffic. Similar to other intracellular trafficking processes, the involvement of microtubules in fusion between autophagosomes and lysosomes is under considerable debate. In this study, we could directly link microtubule-dependent movement with autophagic activity. We showed that mature autophagosomes are associated with microtubules and move along these tracks, yet intact microtubules are not essential for autophagosome targeting and fusion with lysosomes. Previous reports linked microtubules to autophagy. For example, the microtubule toxin vinblastine is commonly used to accumulate autophagosomes in rat hepatocytes (28). However, Kochl *et al.* (27) have recently shown that this accumulation reflects increased autophagosome formation and occurs prior to microtubule depolymerization by vinblastine, indicating that the observed effect is not necessarily related to the microtubule state of polymerization/depolymerization. In accord with our findings, that report has also shown that intact microtubules facilitate autophagosome formation. However, the authors link microtubule depolymerization with inhibition of autophagosome-endosome fusion (27, 30). The different response to microtubule disassembly reported by Kochl *et al.* (27) may be explained by the different cell system or the higher nocodazole concentrations used by these authors. Consistent with these reports, when high concentrations of nocodazole were applied here as in those studies, bulk protein degradation was blocked. We have shown, however, that treatment with low nocodazole concentration, which was sufficient to completely abolish movement of autophagosomes, did not affect targeting and fusion with lysosomes nor did it block bulk protein degradation. Therefore, we suggest that inhibiting autophagy with high concentrations of nocodazole may result from indirect effects on lysosome function.

Functional loss of dynein, a minus end-directed microtubule motor protein, and microtubule disruption by nocodazole (0.1 ng/ml) have been recently linked to impairment in autophagic clearance of aggregate-prone proteins. These studies suggest that dynein mutations and microtubule disruption impair targeting of autophagosomes to lysosomes via microtubules (40, 41). However, these studies applied long periods (at least 48 h) of nocodazole treatment or dynein inactivation. Such conditions inhibited to some degree the basal level of autophagosome targeting and may indicate that microtubules indeed have a marginal effect on autophagosomes targeting to lysosomes, which in our studies could not be detected. The long periods of microtubule-dependent transport inhibition may have an indirect effect on autophagy. We show here that long periods of nocodazole treatment impair degradation of LC3 within lysosomes, possibly by inhibition of the delivery of lysosomal hydrolases as reported previously (42).

The role of microtubules in autophagy is still an open issue. For a mature autophagosome to reach and engage with a distant lysosome, movement is certainly required. A directional delivery along microtubules is the most conceivable route to achieve this engagement. Yet, our results suggest that microtubule-dependent movement is dispensable for autophagy. This may arise from the fact that upon microtubule depolymerization the tight association that exists between lysosomes and microtubules is disrupted, and lysosomes become distributed throughout the cytoplasm. In such a case, and considering the large number of lysosomes, diffusion may be sufficient to allow their engagement with autophagosomes. In the presence of intact microtubules (the normal physiological state), however, lysosomes are concentrated at the microtubule organizing center; therefore, autophagosomes require microtubules for successful targeting. Thus, the existence of autophagosomes and lysosomes on the same tracks (microtubules) allows fusion to occur.

We found that Atg5-labeled phagophores, in contrast to autophagosomes, are immobile organelles. This static nature of phagophores may represent an extra spatial barrier between phagophores and lysosomes that prevents undesirable fusion between these two organelles. Thus it is possible that microtubules play a role in preventing this type of fusion allowing only autophagosomes and lysosomes to move along it but not phagophores. This may explain the reduction in autophagosome formation observed in the absence of intact microtubules.

Finally, our results indicate that the only detectable effect of microtubule disassembly is an ~25% reduction in autophagosome formation. Therefore, we suggest that microtubules facilitate early stages of autophagosome biogenesis. What can be the involvement of microtubules in this stage? Two synchronous ubiquitin-like systems take part in early stages of autophagosome formation. The first is composed of the Atg12-Atg5 conjugate, which together with Atg16 is localized on the phagophore membrane, allowing the conjugation of LC3 to phosphatidylethanolamine on this membrane. LC3 remains on the mature autophagosomes, whereas Atg12-Atg5 and Atg16 are excluded (12). Indeed, LC3 was originally identified as a microtubule-associated factor (15). Consistently, we detected in this study a significant association of this molecule with intact microtubules. It is therefore likely that microtubules facilitate the incorporation of LC3 to the autophagic membrane, leading to increased production of autophagosomes under starvation conditions. Alternatively, microtubules may act downstream to the biogenesis step by facilitating the removal of mature autophagosomes from the production sites. Additional experiments should be addressed to resolve these issues.

Acknowledgments—We thank M. Fainzilber, J. Lowengrub, Y. Avivi, and Y. Barash for discussions and critical evaluation of the manuscript and V. Kiss for technical assistance.

REFERENCES

1. Seglen, P. O., and Bohley, P. (1992) *Experientia* (*Basel*) **48,** 158–172
2. Tanida, I., Tanida-Miyake, E., Komatsu, M., Ueno, T., and Kominami, E. (2002) *J. Biol. Chem.* **277,** 13739–13744
3. Noda, T., Suzuki, K., and Ohsumi, Y. (2002) *Trends Cell Biol.* **12,** 231–235
4. Levine, B., and Klionsky, D. J. (2004) *Dev. Cell* **6,** 463–477
5. Ohsumi, Y. (2001) *Nat. Rev. Mol. Cell Biol.* **2,** 211–216
6. Klionsky, D. J., Cregg, J. M., Dunn, W. A., Jr., Emr, S. D., Sakai, Y., Sandoval, I. V., Sibirny, A., Subramani, S., Thumm, M., Veenhuis, M., and Ohsumi, Y. (2003) *Dev. Cell* **5,** 539–545
7. Tsukada, M., and Ohsumi, Y. (1993) *FEBS Lett.* **333,** 169–174
8. Thumm, M., Egner, R., Koch, B., Schlumpberger, M., Straub, M., Veen-

huis, M., and Wolf, D. H. (1994) *FEBS Lett.* **349,** 275–280
9. Harding, T. M., Morano, K. A., Scott, S. V., and Klionsky, D. J. (1995) *J. Cell Biol.* **131,** 591–602
10. Mizushima, N., Yamamoto, A., Hatano, M., Kobayashi, Y., Kabeya, Y., Suzuki, K., Tokuhisa, T., Ohsumi, Y., and Yoshimori, T. (2001) *J. Cell Biol.* **152,** 657–668
11. Kuma, A., Hatano, M., Matsui, M., Yamamoto, A., Nakaya, H., Yoshimori, T., Ohsumi, Y., Tokuhisa, T., and Mizushima, N. (2004) *Nature* **432,** 1032–1036
12. Mizushima, N., Kuma, A., Kobayashi, Y., Yamamoto, A., Matsubae, M., Takao, T., Natsume, T., Ohsumi, Y., and Yoshimori, T. (2003) *J. Cell Sci.* **116,** 1679–1688
13. Kirisako, T., Ichimura, Y., Okada, H., Kabeya, Y., Mizushima, N., Yoshimori, T., Ohsumi, M., Takao, T., Noda, T., and Ohsumi, Y. (2000) *J. Cell Biol.* **151,** 263–276
14. Ichimura, Y., Kirisako, T., Takao, T., Satomi, Y., Shimonishi, Y., Ishihara, N., Mizushima, N., Tanida, I., Kominami, E., Ohsumi, M., Noda, T., and Ohsumi, Y. (2000) *Nature* **408,** 488–492
15. Mann, S. S., and Hammarback, J. A. (1994) *J. Biol. Chem.* **269,** 11492–11497
16. Wang, H., Bedford, F. K., Brandon, N. J., Moss, S. J., and Olsen, R. W. (1999) *Nature* **397,** 69–72
17. Sagiv, Y., Legesse-Miller, A., Porat, A., and Elazar, Z. (2000) *EMBO J.* **19,** 1494–1504
18. Kabeya, Y., Mizushima, N., Ueno, T., Yamamoto, A., Kirisako, T., Noda, T., Kominami, E., Ohsumi, Y., and Yoshimori, T. (2000) *EMBO J.* **19,** 5720–5728
19. Kabeya, Y., Mizushima, N., Yamamoto, A., Oshitani-Okamoto, S., Ohsumi, Y., and Yoshimori, T. (2004) *J. Cell Sci.* **117,** 2805–2812
20. Tanida, I., Tanida-Miyake, E., Ueno, T., and Kominami, E. (2001) *J. Biol. Chem.* **276,** 1701–1706
21. Tanida, I., Komatsu, M., Ueno, T., and Kominami, E. (2003) *Biochem. Biophys. Res. Commun.* **300,** 637–644
22. Scherz-Shouval, R., Sagiv, Y., Shorer, H., and Elazar, Z. (2003) *J. Biol. Chem.* **278,** 14053–14058
23. Mizushima, N., Yamamoto, A., Matsui, M., Yoshimori, T., and Ohsumi, Y. (2004) *Mol. Biol. Cell* **15,** 1101–1111
24. Bampton, E. T., Goemans, C., Niranjan, D., Mizushima, N., and Tolkovsky, A. M. (2005) *Autophagy* **1,** 23–36
25. Fengsrud, M., Roos, N., Berg, T., Liou, W., Slot, J. W., and Seglen, P. O. (1995) *Exp. Cell Res.* **221,** 504–519
26. Punnonen, E. L., and Reunanen, H. (1990) *Exp. Mol. Pathol.* **52,** 87–97
27. Kochl, R., Hu, X. W., Chan, E. Y., and Tooze, S. A. (2006) *Traffic* **7,** 129–145
28. Seglen, P. O., Berg, T. O., Blankson, H., Fengsrud, M., Holen, I., and Stromhaug, P. E. (1996) *Adv. Exp. Med. Biol.* **389,** 103–111
29. Reunanen, H., Marttinen, M., and Hirsimaki, P. (1988) *Exp. Mol. Pathol.* **48,** 97–102
30. Aplin, A., Jasionowski, T., Tuttle, D. L., Lenk, S. E., and Dunn, W. A., Jr. (1992) *J. Cell Physiol.* **152,** 458–466
31. Mousavi, S. A., Kjeken, R., Berg, T. O., Seglen, P. O., Berg, T., and Brech, A. (2001) *Biochim. Biophys. Acta* **1510,** 243–257
32. Kovacs, A. L., and Seglen, P. O. (1982) *Acta Biol. Med. Ger.* **41,** 125–130
33. Yamamoto, A., Tagawa, Y., Yoshimori, T., Moriyama, Y., Masaki, R., and Tashiro, Y. (1998) *Cell Struct. Funct.* **23,** 33–42
34. Blommaart, E. F., Krause, U., Schellens, J. P., Vreeling-Sindelarova, H., and Meijer, A. J. (1997) *Eur. J. Biochem.* **243,** 240–246
35. Kihara, A., Kabeya, Y., Ohsumi, Y., and Yoshimori, T. (2001) *EMBO Rep.* **2,** 330–335
36. Seglen, P. O., and Gordon, P. B. (1982) *Proc. Natl. Acad. Sci. U. S. A.* **79,** 1889–1892
37. Musch, A. (2004) *Traffic* **5,** 1–9
38. Ishihara, N., Hamasaki, M., Yokota, S., Suzuki, K., Kamada, Y., Kihara, A., Yoshimori, T., Noda, T., and Ohsumi, Y. (2001) *Mol. Biol. Cell* **12,** 3690–3702
39. Shorer, H., Amar, N., Meerson, A., and Elazar, Z. (2005) *J. Biol. Chem.* **280,** 16219–16226
40. Ravikumar, B., Acevedo-Arozena, A., Imarisio, S., Berger, Z., Vacher, C., O'Kane, C. J., Brown, S. D., and Rubinsztein, D. C. (2005) *Nat. Genet.* **37,** 771–776
41. Webb, J. L., Ravikumar, B., and Rubinsztein, D. C. (2004) *Int. J. Biochem. Cell Biol.* **36,** 2541–2550
42. Scheel, J., Matteoni, R., Ludwig, T., Hoflack, B., and Kreis, T. E. (1990) *J. Cell Sci.* **96,** 711–720
43. Porat, A., and Elazar, Z. (2000) *J. Biol. Chem.* **275,** 29233–29237
44. Hamming, R. W. (1991) *The Art of Probability for Scientist and Engineers*, pp. 145–146, Addison-Wesley, Redwood City, CA